Journal of The Electrochemical Society

Mechanism and Kinetics of Na_2S_x ($x \leq 2$) Precipitation in Sodium-Sulfur and Sodium/(Oxygen)-Sulfur Batteries

To cite this article: Qipeng Zhang *et al* 2024 *J. Electrochem. Soc.* **171** 010503

Journal of The Electrochemical Society, 2024 171 010503

Mechanism and Kinetics of Na_2S_x ($x \leqslant 2$) Precipitation in Sodium-Sulfur and Sodium/(Oxygen)-Sulfur Batteries

Qipeng Zhang, Tairan Yang, and Zheng Li[z]

Department of Mechanical Engineering, Virginia Polytechnic Institute and State University, Blacksburg, Virginia 24061, United States of America

Room-temperature sodium-sulfur (RT Na-S) batteries have attracted ever-increasing attention because of their enhanced energy density and low price. Although the performance of RT Na-S batteries is obtained in many other research, the basic mechanism and kinetics have not involved yet, especially in discharge product growth, which affects electrochemical performance. Meanwhile, designed additional redox activities (in the presence of oxygen) could simultaneously suppress sodium polysulfide shuttling and enhance energy density according to our group reported. However, the kinetic study of the intermediate has not been explored. In this work, we discussed the deposition of low-order sodium polysulfide (Na_2S_x, $x \leqslant 2$) in different potentials and types of glyme-solvents in Na-S and Na/(O_2)-S system. The results show that the morphology of deposition Na_2S_x ($x \leqslant 2$) is affected by interfacial energy barrier controlled by overpotentials and the radius of sodium ions, which produced the precipitation of particle shape rather than film. Potentiostatic experiments show the kinetics are elevated in the presence of oxygen. In addition, the exchange current density of different sodium polysulfides was studied. The high-order sodium polysulfide has a lower exchange current density than that of low-order sodium polysulfide in Na-S system, requiring greater driving force, while transformation of the intermediate from high-order oxy-sulfur to low-order oxy-sulfur species require less impulse in Na/(O_2)-S systems. This paper provides new understandings of the deposition mechanism and kinetics of Na_2S_x ($x \leqslant 2$) Na-S and Na/(O_2)-S system in and to choose the appropriate solvent and potential.

 [DOI: 10.1149/1945-7111/ad14cb]

Manuscript submitted September 23, 2023; revised manuscript received November 16, 2023. Published January 3, 2024.

Supplementary material for this article is available online

Low cost, high energy-density electrochemical energy storage technology is critical for development of electric vehicles (EVs) and power grids.[1] The development of lithium-sulfur (Li-S) batteries with a lithium-metal anode and a sulfur cathode has received a lot of attention over the past ten years because of their high theoretical capacity of 1675 mA h g^{-1}. However, due to a paucity of lithium resources (0.0065% of the Earth's crust), Li-S batteries are prohibitively expensive and especially impractical for grid-scale energy storage applications.[2–10] Therefore, it is urgent to explore and develop a new alternative battery system. Room-temperature sodium-sulfur (RT Na-S) batteries are garnering more attention due to their low price ($50–100 kWh^{-1}), abundant source of elements (2.7% of the Earth's crust is sodium), and same theoretical capacity (1675 mAh g^{-1} when Na-S battery is fully converted to Na_2S).[11–14] RT Na-S and Li-S batteries are chemically similar, but not identical. Both of them mainly undergo multi-step reactions between the metal anode and S cathode, which is a typical multi-platform phenomenon in the discharge profile. However, the discharge behaviors are actually different, which might be due to the inherent differences between sodium and lithium. Compared to the lithium ion, sodium ion has a larger radius, which means that the kinetics is more sluggish, especially in solid-phase conversion reaction, and volume expansion is significant (260% from S to Na_2S). Moreover, discharge products of high-order sodium polysulfides are more soluble in liquid electrolytes.[15–17] Therefore, in the past decades, people have been trying to find electrode and electrolytes suitable for sodium ion embedding, and have successfully develop many new Na-based materials and solvents, achieving high energy-density. For instance, Jiang et al. developed sulfur-doped disordered carbon. The advantageous inclusion of sulfur into the carbon structure may offer more reaction sites for Na^+ accommodation. Benefiting from this design, the Na-S batteries exhibited outstanding performances with a specific capacity of 271 mAh g^{-1} at 1 A g^{-1} after 1000 cycles.[18] Our group proposed a new hybrid strategy using oxygen in sodium sulfur system, which alter the underlying reaction pathway, achieving a high discharge capacity of over 1400 mAh g^{-1}.[19] Although these mentioned RT Na-S batteries show better electrochemical performance, Na_2S_x ($x \leqslant 2$) growth in RT Na-S battery has not been systematically elucidated.[20–22]

Herein, the kinetics and morphology of electrodeposition of Na_2S_x ($x \leqslant 2$) on carbon surface with three glyme-based polysulfide solutions in Na-S and Na/(O_2)-S batteries were studied. For Na-S system, the deposition mechanism of Na_2S_x ($x \leqslant 2$) was determined by kinetic analysis and direct observation of the morphology of Na_2S_x ($x \leqslant 2$) in different deposition times. The results show that the morphology of electrodeposited Na_2S_x ($x \leqslant 2$) depends on the nucleation density and the relative rate of nucleation and growth, which can be controlled by the selection of overpotential and solvent in Na-S system, and the sediment is shaped as a particle rather than a film. However, the deposition of discharge products is solvent-sensitive but seems to be less sensitive to overpotential in system Na/(O_2)-S system. In addition, the exchange current densities of different high-order polysulfide compounds were also evaluated. The results show that the exchange current density of high-order sodium polysulfide solution is lower than that of low-order sodium polysulfide solution for system in the absence of oxygen, which means that the driving force required is larger. Meanwhile, we found, compared with the Na-S system, when the high-order goes to the low-order sodium polysulfide, less drive is needed in Na/(O_2)-S. This work provides a way to understand the deposition of Na_2S_x ($x \leqslant 2$).

Experimental

Preparation of materials.—Sodium polysulfide (Na_2S_x, $4 \leqslant x \leqslant 8$) solution was prepared by stirring 0.5 M sodium trifluoromethanesulfonate ($NaSO_3CF_3$, Alfa Aesar) in Diglyme, Triglyme, and Tetraglyme electrolyte first, and then 1.5 M sodium sulfide (Na_2S, 99%, Alfa Aesar) and 4.5, 6.0, 7.5, 9.0, 10.5 M sulfur (Alfa Aesar), respectively were added into electrolytes at 60 °C for 8 h. The total sulfur concentration in the polysulfide solution was 1.5 M. The electrolyte was dried on molecular sieves for 7 d. The $NaSO_3CF_3$ salt was dried under vacuum at 120 °C for 8 h.

[z]E-mail: zhengli@vt.edu

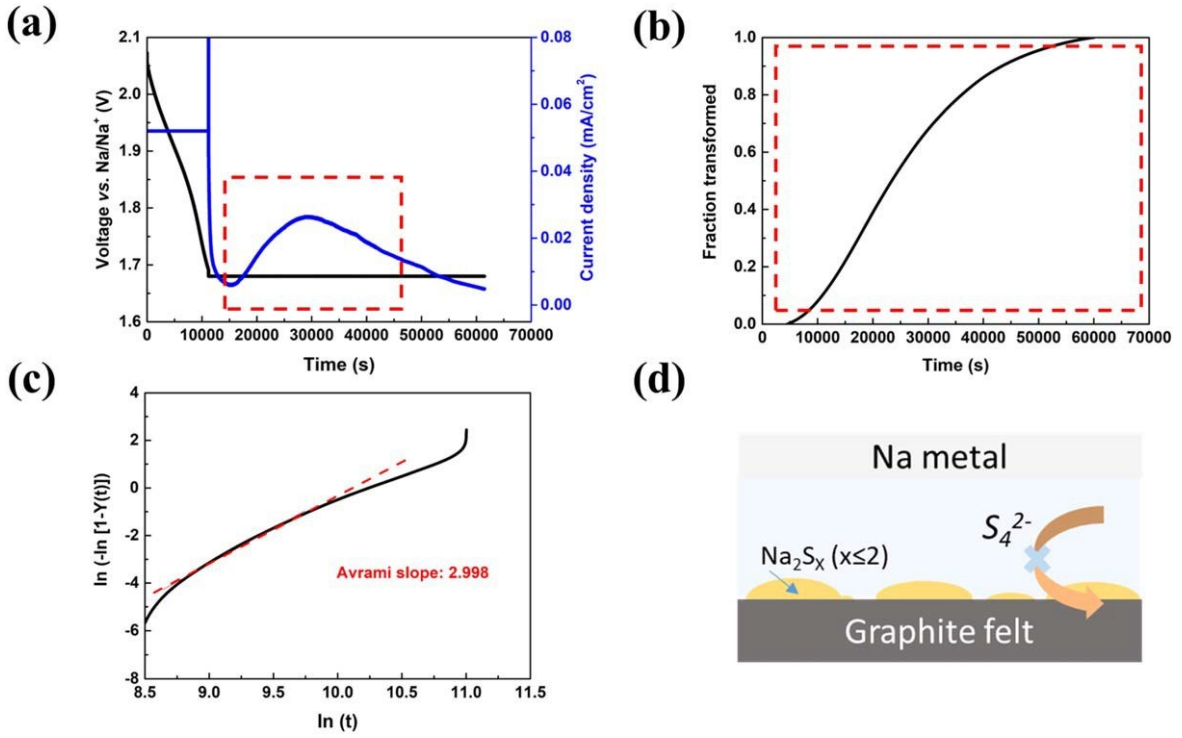

Figure 1. (a) Voltage and current density vs time for a baseline Na-S cell, which was first galvanostatically discharged to 1.70 V and then potentiostatically discharged at 1.68 V. (b) Transformation vs time plot for potentiostatic current peak (enclosed in red in (a)). (c) Avrami plot resulting from the boxed portion of (b). (d) Proposed mechanism for the reduction of sodium polysulfides.

Potentiostatic experiments.—Graphite felt with a diameter of 14 mm and thickness of 1–1.5 mm was used as a working electrode. Na polysulfide (nominal Na_2S_6) solution of 40 uL was uniformly dropped on the graphite felt. The sulfur loading was calculated to be around 1.25 mg cm^{-2}. Na metal was used as a counter/reference electrode, and glass microfiber filters (GF/D, Whatman) were used to separate the electrode. All Na-S cells were performed in CR2032-type coin cells in an argon-filled glovebox (O_2 < 0.1 ppm, H_2O < 0.1 ppm). The Na/(O_2)-S cell, the coin cell with 4 side holes, was assembled and tested in the oxygen-filled box. The cells were first discharged galvanostatically. Subsequently, a potentiostatic experiment was carried out where the potential was held at different voltages (1.64, 1.66, 1.67, and 1.68 V) for the reduction of polysulfides.

Electrochemical impedance spectroscopy measurements.—EIS measurements were performed by Bio-Logic SP-150 potentiostat. All sodium polysulfide solution was taken within Tetraglyme with 0.5 M $NaSO_3CF_3$ supporting electrolyte. Na-S cells were measured using a 5-mV amplitude over a frequency ranging from 100 kHz to 10 mHz.

Exchange current density measurements.—In the galvanostatic polarization experiment, a specified current was drawn from the H-cell using a 3 mm glassy carbon working electrode (CH Instruments, Inc.). The corresponding potential was determined as the average during the 30-minute galvanostatic step. For the Na/(O_2)-S cell, the H-cell was tested in the oxygen-filled box.

Microscopy characterization.—SEM of the graphite felt was carried out using JSM-IT500HR SEM (JEOL, Peabody, MA, USA).

Results and Discussion

Mechanism and kinetics in Na-S systems.—In the potentiostatic experiment, a constant driving force (i.e., overpotential) was provided, and the time evolution of sulfur reduction was monitored by constant current so that the potential was kept below the equilibrium potential (determined at 1.805 V in the electrolytic cell; see Fig. S1, supporting information). Starting solutions consisted of 1.5 M Na_2S_6 as the sulfur source, dissolved in three different solvents (Diglyme, Triglyme, and Tetraglyme, respectively) with 0.5 M sodium trifluoromethanesulfonate ($NaSO_3CF_3$) as a supporting sodium salt (glyme-based ether solvents are typically used in electrolytes, which provide the exceptional reversibility in Na-S batteries). When the Na-S battery was discharged, several polysulfides can coexist in the electrolyte in a balanced and reduced state. To distinguish the electrodeposition of Na_2S_x ($x \leqslant 2$) from the reduction of Na_2S_4 or higher order sodium polysulfides (i.e., Na_2S_6) in solution, each cell was initially discharged with a continuous current at a C/24 rate to a potential of 1.7 V. The potential was then sustained at various voltages (between 1.64 and 1.68 V vs Na/Na^+) for the reduction of polysulfides in a subsequent potentiostatic experiment.

Figure S2 depicts the change in voltage and current as well as how the evolution of polysulfide reduction through time was captured via the current flow. Using Tetraglyme electrolyte as an example, the progressive conversion of higher-order polysulfide (Na_2S_x, $x \geqslant 4$) into Na_2S_4 in the solution causes the voltage to fall monotonically throughout the initial galvanostatic discharge process. Around 12000 seconds into the potentiostatic discharge, a sharp reduction in current is observed. This is a result of lowering the remaining higher-order sodium polysulfides (Na_2S_x, $x \leqslant 4$). The nucleation of Na_2S_x ($x \leqslant 2$) and its growth to impingement cause a current peak to follow that.[23] The reduction of Na_2S_6 and Na_2S_4 (blue and red, respectively), as well as a peak brought on by the electrodeposition of Na_2S_x ($x \leqslant 2$), are represented by the curve (in red) in Fig. S3. Because Na_2S_6 has a higher equilibrium potential for reduction than Na_2S_4, the former species has a greater overpotential for reduction and, as a result, a larger initial current. Additionally, because of the relative lower concentration, the decrease current of the former species quickly diminishes. The current then asymptotically approaches zero, which is attributable to the deposition of

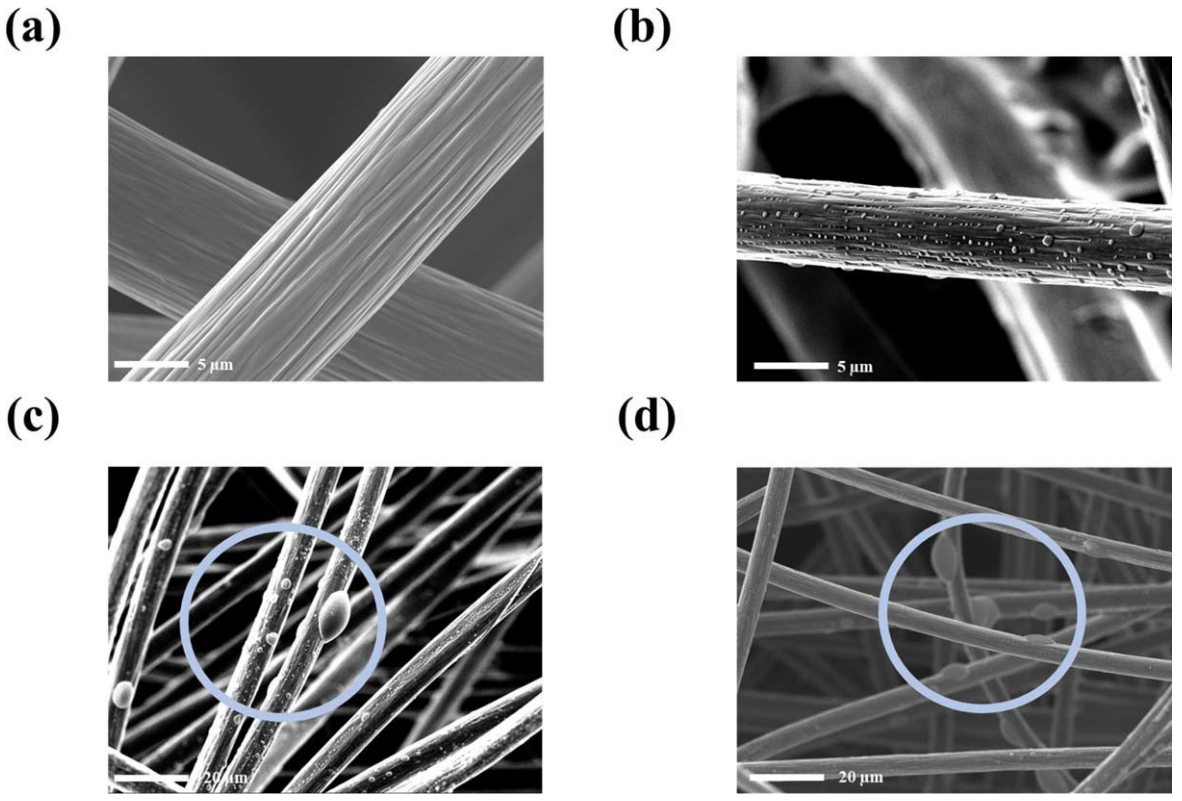

Figure 2. (a) SEM image of pristine graphite felt. SEM images after (b) 1 h, (c) 2 h, and (d) 3 h.

Na_2S_x ($x \leqslant 2$) effectively ceasing. Next, the behavior characteristics of the two-dimensional island nucleation and growth (precipitation) process were releveled. The background fitting of the current-time curve was performed using the sum of two exponential functions, and the peaks were isolated by the subtraction of the exponential functions (Fig. 1a). The current peak value is a sigmoidal cumulative distribution function (Fig. 1b), and its distribution obeys Avrami form (Eq. 1):[24]

$$Y(t) = 1 - \exp(-\pi A K^2 t^n/3) \quad [1]$$

where Y is the fraction of the material that has been transformed, n is the Avrami exponent, and A and k are the nucleation and growth rates, respectively. Both Ak^2 and n are related to the dimensionality of growth.[25] Fitting the data with Eq. 1 (Fig. 1c) gives an Avrami exponent of 2.998 (close to 3), consistent with progressive nucleation.[26]

The dimension and deposition morphology anticipated from kinetic analysis were confirmed by direct scanning electron microscopy (SEM) imaging. Figure 2a shows the measured potentiostatic deposition curve and the image of the pristine carbon fiber.

The discharge products are relatively tiny and evenly dispersed due to a minimal initial overpotential. The overpotential increases continuously with the addition of deposition time, resulting in a higher surface energy barrier to absorb S_4^{2-} and the formation of new nuclei. Thus, the growth of Na_2S_x ($x \leqslant 2$) is restricted. When the deposition time is 2 or 3 h, deposition of Na_2S_x ($x \leqslant 2$) is mainly development, accompanied by other new nuclei formed. Chiang's group studied the morphology of Li_2S electrodeposited on carbon-based materials by glyme-based non-aqueous polysulfide solution.[27] They discovered that the electrodeposited Li_2S has the shape of a thin 2D film. Unlike the deposition of lithium sulfide, the radius of sodium ion is much larger than that of lithium-ion, and the insufficient surface area also makes the deposition of deposition of Na_2S_x ($x \leqslant 2$) not as uniform as that of lithium sulfide.[28,29] Thus, the precipitation of particle shape to the Na_2S_x ($x \leqslant 2$) rather than film. It is also worth noting that the incomplete Na_2S_x ($x \leqslant 2$) transformation also affects the precipitation, but the kinetics of the surface reaction mainly limits this. Meanwhile, additional experiments were performed to verify that the chemical transformation of Na_2S_x ($x \leqslant 2$) must be limited by the kinetics of the surface reaction rather than by the supply of sulfur or mass transfer to the growth interface. Cyclical voltammetry (CV) was utilized to examine the possibility of a mass transport constraint. In the 19000 s experiment, where the diffusion length is more than 1 mm, the diffusion coefficient of Na_2S_x is 9.37 10^{-7} cm^2 s^{-1}, as shown in Fig. S4. Mass migration of the polysulfide to the deposition site cannot be prevented if the distance between electrode fibers is about 20 μm (Fig. S5, supporting information).

Based on the above morphological and kinetic observations, we proposed the possible growth mechanism of Na_2S_x ($x \leqslant 2$), as shown in Fig. 1d. We believe the Na_2S_x ($x \leqslant 2$) deposition was characterized by relatively tiny and homogeneous particles because of the initial nucleation density and minimal overpotential. However, the interfacial energy barrier starts to increase as precipitation time increases. Since the surface area is confined and the sodium ion is large, more new locations cannot be found to continue depositing and expanding. Therefore, particles comprise most of the Na_2S_x ($x \leqslant 2$) deposition. Additionally, because Na_2S_x ($x \leqslant 2$) has a very low conductivity, it is difficult for the reaction to proceed when deposited on the graphite felt surface. As a result, the final current decreases until it almost reaches zero.

By performing the potentiostatic discharge at different voltages in tretaglyme electrolytes, the nucleation-growth rate constant could also be calculated at different voltages. In Fig. 3a, the initial Na-S cells were galvanostatically discharged to 1.70 V at a rate of C/24, and subsequently they were potentiostatically discharged at 1.68, 1.67, 1.66, and 1.64 V. The reduction of current provides a greater overpotential for the electrodeposition process. Therefore, the deposition rate of Na_2S_x ($x \leqslant 2$) is significantly increased. Meanwhile, potentiostatic discharge at different voltages using two other ether-based solvents were also performed as shown in Figs. 3b

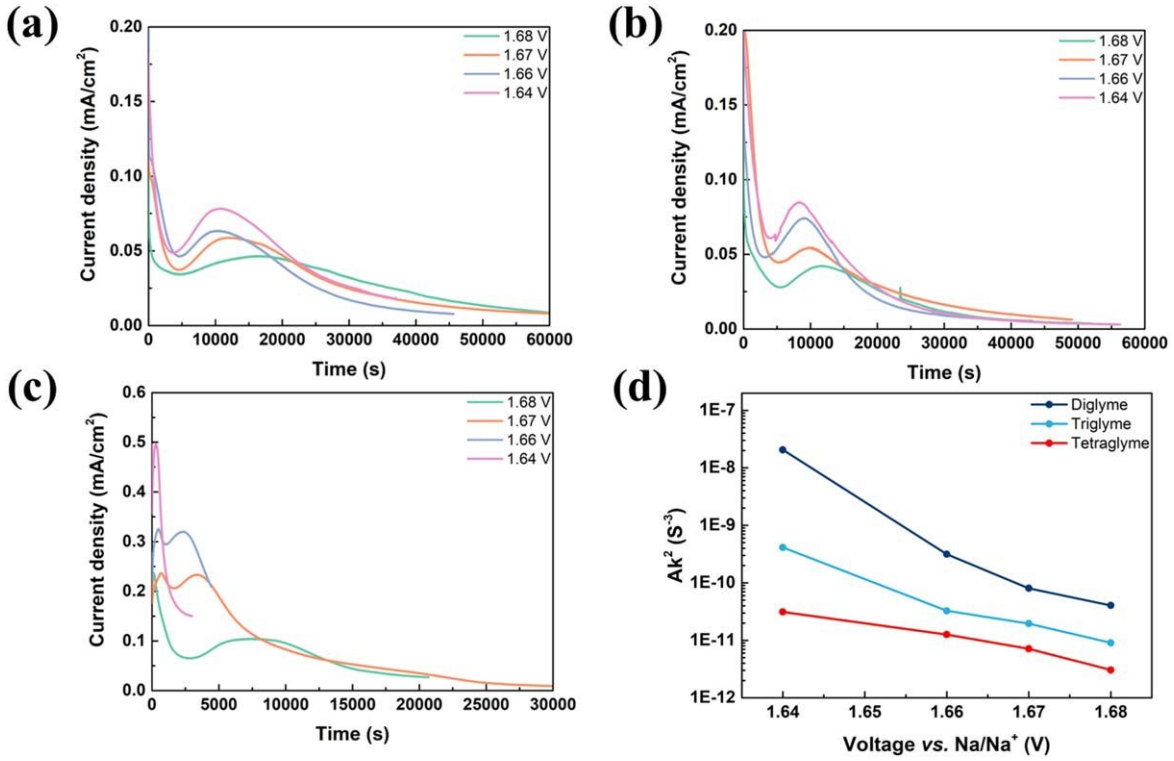

Figure 3. Current-time diagrams of potentiostatic discharge in different solvents: (a) Tetraglyme, (b) Triglyme, and (c) Diglyme. (d) Combined nucleation-growth rate constants obtained from current peak fitting.

and 3c. When the solvent was changed to Triglyme or Diglyme, the deposition rate of Na_2S_x ($x \leqslant 2$) increases significantly, which may be due to the chain lengths of Triglyme and Diglyme significantly decreasing compared with the Tetraglyme. As the length decreases, the number of oxygen molecules decreases, as well as the viscosity. In addition, the viscosity of the solvent also affects the diffusion rate of sodium ions. CV curves of 1 M Na_2S_6 in three different solvents with different sweep speeds were obtained in Fig. S6. The diffusion rate of sodium ions in three different solvents is Diglyme > Triglyme > Tetraglyme. This demonstrates sodium ions can continuously replenish themselves in the solvent Diglyme and react on the graphite felt surface. Subsequent deposition occurs at a faster rate as a result. It is worth noting that the Diglyme electrolyte showed two current peaks. Tetraglyme is about four times as viscous as Diglyme, it is thought that the first peak was caused by the electrodeposition of Na_2S_x ($x \leqslant 2$) from higher-order polysulfides that had not yet completely reduced to Na_2S_4 during the galvanostatic discharge process.[30] Therefore, the second current peak in the curve was used for fitting and calculating the nucleation-growth rate constant. Figure 3d shows the nucleation-growth rate constants at different voltages. Increased nucleation-growth rate constants are seen because the electrodeposition process has a greater overpotential due to the voltage drop. When the voltage drops to 1.64 V, this rise is extremely apparent (even two orders of magnitude greater). This resembles the pattern of Li_2S deposition on the surface of carbon. [27]

Furthermore, different concentrations of Na_2S_6 (1.5, 2.0, and 2.5 M respectively) into the three electrolytes to evaluate deposition kinetics were also discussed, and the results were shown in the Fig. 4. As the concentration of sodium polysulfide in Tetraglyme electrolyte increases, it is clear that the deposition rate increases as well. This might be the case because concentration increases the chance of a direct collision between the reactants, which speeds up the reaction's rate and process. In the meantime, due to the distinct properties of the two additional ether-based solvents used in place of Tetraglyme for potentiostatic discharge, the deposition rate of Na_2S_x ($x \leqslant 2$) increased. It is noteworthy that, in contrast to the other two ethers, Diglyme does not appear to exhibit a clear rise in rate with concentration.

The exchange current density measurement was used independently to test the Butler-Volmer kinetics at the carbon-solution interfaces, helping us understand the impedance contributions of various polysulfides and calculate overpotentials.[31] Figure 5 depicts using three-electrode cells in Tetraglyme solvent to perform galvanostatic polarization at a glassy carbon macroelectrode to study the kinetics of Na_2S_6 at "model" carbon surfaces. By retracing the linear segment of the Tafel diagram back to the intercept at the equilibrium potential, the exchange current density was calculated. The exchange current density of Na_2S_6 is calculated to be 0.019 mA cm^{-2}. Table I and Fig. S7 summarize the exchange current densities measured from Na_2S_8 to Na_2S_4 solutions. The exchange current densities of Na_2S_8, Na_2S_7, Na_2S_6, Na_2S_5, and Na_2S_4 are 0.011, 0.014, 0.019, 0.021, and 0.024 mA cm^{-2} respectively. An increasing exchange current indicates a rapid exchange of substances, which means the reaction encounters little resistance as it changes. We performed EIS tests to verify the above interpretation (Fig. S8). The results of the measurements of the exchange of current density agree with the conclusions that Na_2S_8 has the highest impedance. The lowest exchange current density is seen in Na_2S_8, which has more reaction steps than lower-order Na_2S_x. As a result, the reaction requires the most energy (i.e., driving force).

Kinetics in Na/(O_2)-S systems.—According to our previous research,[19] NaO_2-Na_2S_n ($4 < n \leqslant 8$) was formed through combining Na^+, O^{2-}, and S_n^{2-} ($4 < n \leqslant 8$) at the stage of the discharge process when the oxygen was present, which may prevent the polysulfides from diffusing to the sodium side, improving the electrochemical performance. However, the kinetic study of the intermediate has not been explored. In this part we investigate interfacial kinetics during the electrochemical reactions in the Na/(O_2)-S system using

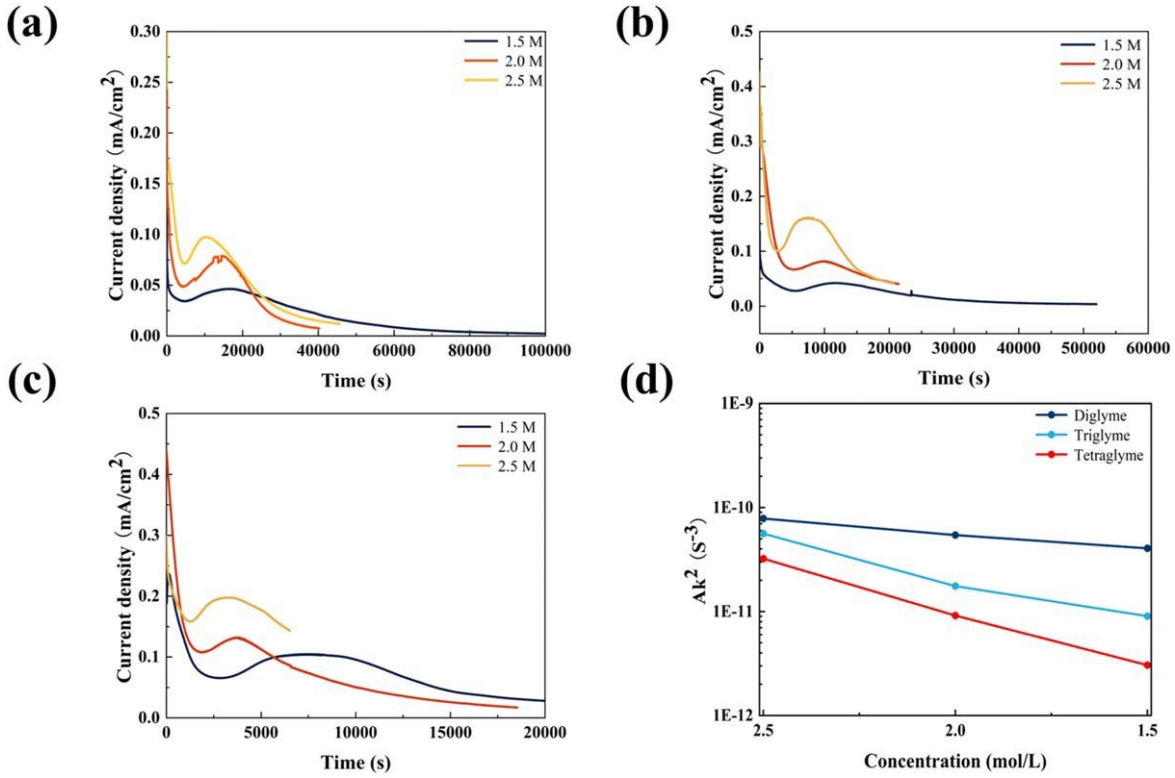

Figure 4. Current-time diagrams of potentiostatic discharge at varied Na_2S_6 concentrations in different solvents: (a) Tetraglyme, (b) Triglyme, and (c) Diglyme. (d) Combined nucleation-growth rate constants obtained from current peak fitting.

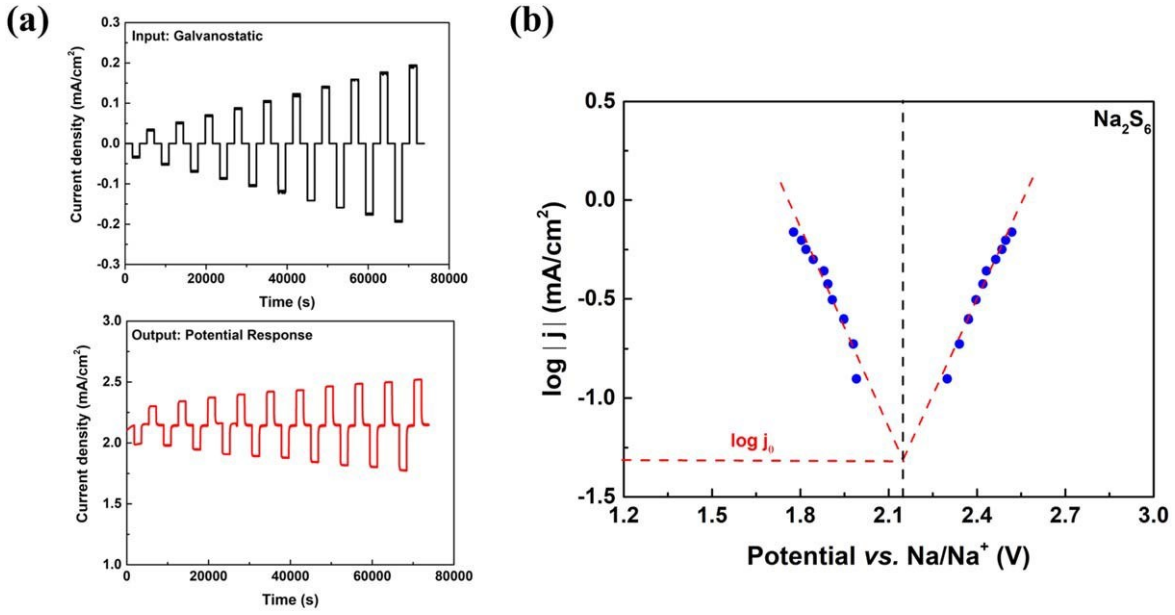

Figure 5. In the galvanostatic polarization experiment, a 3 mm glass carbon working electrode was used to extract the specified current from the cell for 30 min. The corresponding potential is the average potential of 30 min constant current step (a). The Tafel plot of galvanostatic polarization measurements of electrochemical kinetics in 1.5 M Na_2S_6 solutions in Tetraglyme with 0.5 M $NaSO_3CF_3$ supporting electrolyte. The linear extrapolations are shown as line position of the dashed vertical line indicates the dashed lines and the open-circuit voltage (b).

potentiostatic and exchange current density experiments. The results are shown in Fig. 6. There is no significant difference in the shape of the curves at the same voltages compared with Na-S system. The biggest differences are in the deposition time and the magnitude of the current density. The deposition time and current intensity of Na/(O_2)-S systems are greater than those of Na/S systems in different three solvents, indicating that the kinetics are elevated in the presence of oxygen (this was proved by calculating nucleation-growth rate constants at different voltages shown in Fig. 6d). It is also noted that the intermediate appears to be more dependent on the viscosity, while it does not seem sensitive to the increase in voltages. When the solution was changed from Triglyme to Diglyme at

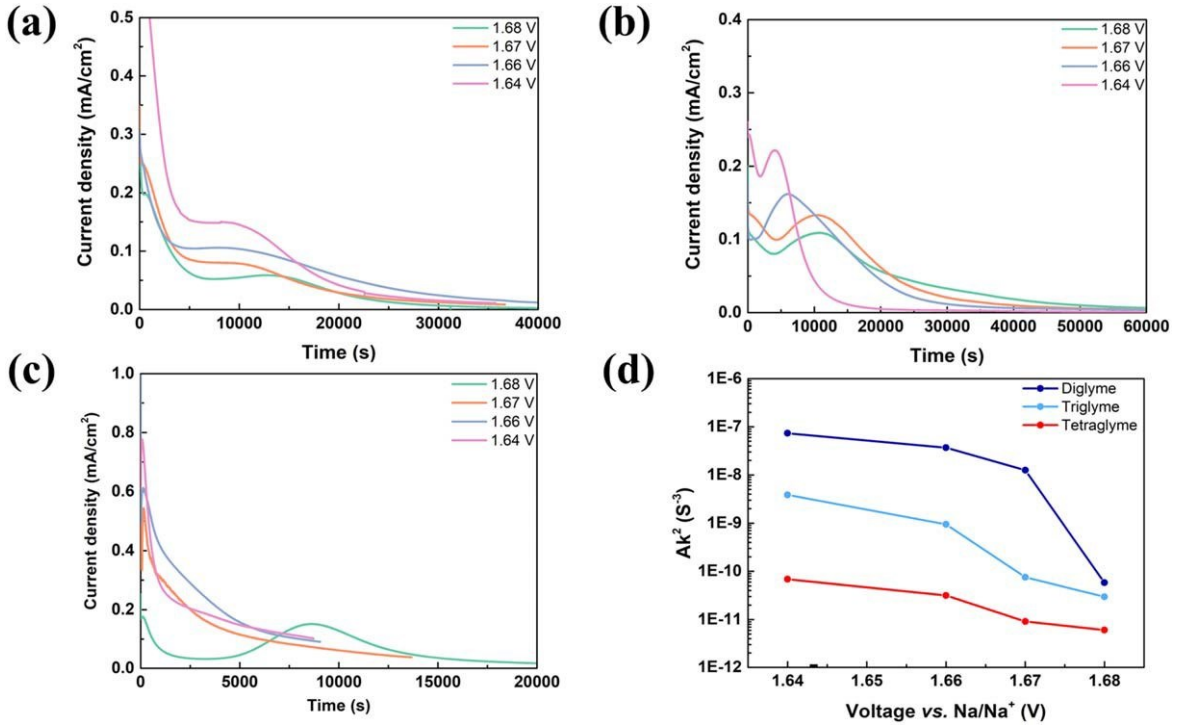

Figure 6. Current–time diagrams of potentiostatic discharge in different solvents in the Na/(O_2)-S system: (a) Tetraglyme, (b) Triglyme, and (c) Diglyme. (d) Combined nucleation-growth rate constants.

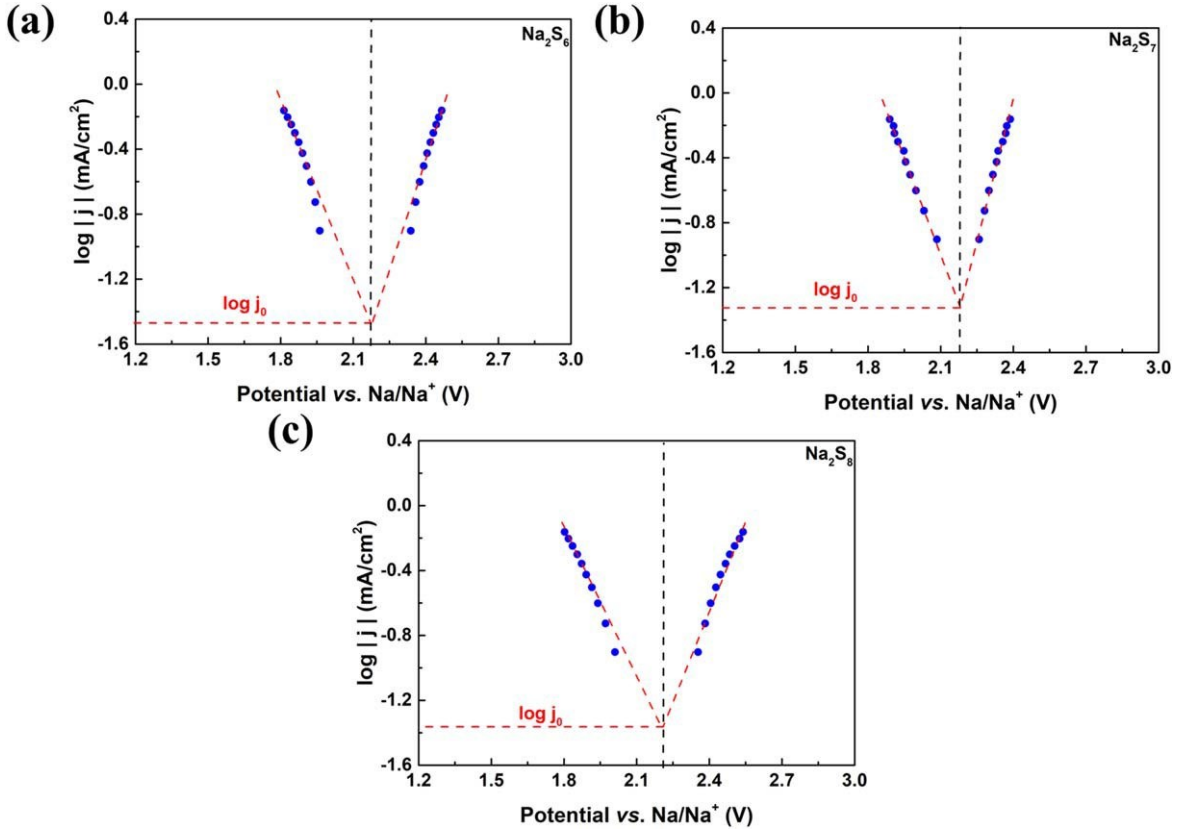

Figure 7. (a) The Tafel plot of galvanostatic polarization measurements of electrochemical kinetics in 1.5 M Na_2S_6, Na_2S_7, and Na_2S_8 solutions in Tetraglyme. The linear extrapolations are shown as the dashed lines, and the open-circuit voltage is indicated by the position of the dashed vertical line.

Table I. Summary of measured exchange current densities in Na/S systems.

Composition	Exchange current density (mA cm^{-2})
1.5 M Na_2S_8	0.011
1.5 M Na_2S_7	0.014
1.5 M Na_2S_6	0.019
1.5 M Na_2S_5	0.021
1.5 M Na_2S_4	0.024

Table II. Summary of measured exchange current densities in $Na/(O_2)$-S systems.

Composition	Exchange current density (mA cm^{-2})
1.5 M Na_2S_8	0.024
1.5 M Na_2S_7	0.025
1.5 M Na_2S_6	0.027

1.66 V, the constant's value increased by a factor of 100 in the $Na/(O_2)$-S system as opposed to simply by a factor of 10 in the Na/S system. When we reduced the voltage at Diglyme solution from 1.66 V to 1.64 V, we discovered no appreciable change in the constant but a 100-fold rise in comparison to the Na/S system.

Exchange current density measurement was also conducted to understand estimate overpotentials. Figure 7 shows the galvanostatic polarization of different sodium polysulfide measured in Tetraglyme solvent when the oxygen exists. The exchange current density was also calculated. Table II summarizes the exchange current densities from Na_2S_8 to Na_2S_6 species. The exchange current densities of Na_2S_8, Na_2S_7, and Na_2S_6 are 0.024, 0.025, and 0.027 mA cm^{-2} respectively. Compared with the Na/S system, the exchange current density is greater than the based one, which indicates a fast exchange of substances NaO_2-Na_2S_n formed, meaning that less resistance is required for the reaction. It is important to note that when the sulfur source was changed from Na_2S_8 to Na_2S_6, the exchange current density changes only slightly. This means that, in comparison to Na_2S_x in Na-S systems, less impulse is needed to convert the intermediate from high-order (NaO_2-Na_2S_n, $4 \leqslant n \leqslant 8$) to low-order ($NaO_2$-$Na_2S_n$, $n < 4$) species.

Conclusions

In summary, we studied the deposition of Na_2S_x ($x \leqslant 2$) in different potentials and solvents with/without oxygen. The results show that the deposit of Na_2S_x ($x \leqslant 2$) was mainly controlled by overpotential and solvent in the Na-S system. The effect of the interface barrier regulated by overpotentials and the larger sodium ion radius compared with lithium-ion cause the electrochemical deposition to take the shape of a particle rather than a film. For the $Na/(O_2)$-S system, oxy-sulfur species are mainly affected by solvent. In addition, the effect of different sodium polysulfides on the exchange current density is also discussed. The results showed that the higher-order sodium polysulfide had the lowest current density, meaning that it needed a more significant push to react. Transformation of the intermediate from high-order oxy-sulfur to low-order oxy-sulfur components needs lesser driving force in $Na/(O_2)$-S than Na-S systems. This paper provides an insight into the mechanism of Na_2S_x ($x \leqslant 2$) deposition and a new idea for selecting suitable solvents and potentials.

ORCID

Zheng Li https://orcid.org/0000-0002-6842-9052

References

1. D. Larcher and J.-M. Tarascon, "Towards greener and more sustainable batteries for electrical energy storage." *Nat. Chem.*, 7, 19 (2015).
2. B. Dunn, H. Kamath, and J.-M. Tarascon, "Electrical energy storage for the grid: a battery of choices." *Science*, 334, 928 (2011).
3. N. Nitta, F. Wu, J. T. Lee, and G. Yushin, "Li-ion battery materials: present and future." *Mater. Today*, 18, 252 (2015).
4. J. B. Goodenough and K.-S. Park, "The Li-ion rechargeable battery: a perspective." *J. Am. Chem. Soc.*, 135, 1167 (2013).
5. S. Zhang, H. Shi, J. Tang, W. Shi, Z.-S. Wu, and X. Wang, "Super-aligned films of sub-1 nm Bi2O3-polyoxometalate nanowires as interlayers in lithium-sulfur batteries." *Science China Materials*, 64, 2949 (2021).
6. H. Shi, J. Qin, P. Lu, C. Dong, J. He, X. Chou, P. Das, J. Wang, L. Zhang, and Z. S. Wu, "Interfacial engineering of bifunctional niobium (V)-based heterostructure nanosheet toward high efficiency lean-electrolyte lithium–sulfur full batteries." *Adv. Funct. Mater.*, 31, 2102314 (2021).
7. Y. Boyjoo, H. Shi, Q. Tian, S. Liu, J. Liang, Z.-S. Wu, M. Jaroniec, and J. Liu, "Engineering nanoreactors for metal–chalcogen batteries." *Energy Environ. Sci.*, 14, 540 (2021).
8. Y. Boyjoo, H. Shi, E. Olsson, Q. Cai, Z. S. Wu, J. Liu, and G. Q. Lu, "Molecular-level design of pyrrhotite electrocatalyst decorated hierarchical porous carbon spheres as nanoreactors for lithium–sulfur batteries." *Adv. Energy Mater.*, 10, 2000651 (2020).
9. H. Shi, X. Zhao, Z.-S. Wu, Y. Dong, P. Lu, J. Chen, W. Ren, H.-M. Cheng, and X. Bao, "Free-standing integrated cathode derived from 3D graphene/carbon nanotube aerogels serving as binder-free sulfur host and interlayer for ultrahigh volumetric-energy-density lithium sulfur batteries." *Nano Energy*, 60, 743 (2019).
10. H. Shi, Y. Dong, F. Zhou, J. Chen, and Z.-S. Wu, "2D hybrid interlayer of electrochemically exfoliated graphene and Co(OH)2 nanosheet as a bi-functionalized polysulfide barrier for high-performance lithium–sulfur batteries." *J. Phys.: Energy*, 1, 015002 (2018).
11. A. Y. S. Eng, V. Kumar, Y. Zhang, J. Luo, W. Wang, Y. Sun, W. Li, and Z. W. Seh, "Room-temperature sodium–sulfur batteries and beyond: realizing practical high energy systems through anode, cathode, and electrolyte engineering." *Adv. Energy Mater.*, 11, 2003493 (2021).
12. T. Li, J. Xu, C. Wang, W. Wu, D. Su, and G. Wang, "The latest advances in the critical factors (positive electrode, electrolytes, separators) for sodium-sulfur battery." *J. Alloys Compd.*, 792, 797 (2019).
13. F. Yang, S. M. A. Mousavie, T. K. Oh, T. Yang, Y. Lu, C. Farley, R. J. Bodnar, L. Niu, R. Qiao, and Z. Li, "Sodium-sulfur flow battery for low-cost electrical storage." *Adv. Energy Mater.*, 8, 1701991 (2018).
14. C. Delmas, "Sodium and sodium-ion batteries: 50 years of research." *Adv. Energy Mater.*, 8, 1703137 (2018).
15. D. Kumar, S. K. Rajouria, S. B. Kuhar, and D. K. Kanchan, "Progress and prospects of sodium-sulfur batteries: a review." *Solid State Ionics*, 312, 8 (2017).
16. P. Adelhelm, P. Hartmann, C. L. Bender, M. Busche, C. Eufinger, and J. Janek, "From lithium to sodium: cell chemistry of room temperature sodium-air and sodium-sulfur batteries." *Beilstein J. Nanotechnol.*, 6, 1016 (2015).
17. Y. X. Wang, B. Zhang, W. Lai, Y. Xu, S. L. Chou, H. K. Liu, and S. X. Dou, "Room-temperature sodium-sulfur batteries: a comprehensive review on research progress and cell chemistry." *Adv. Energy Mater.*, 7, 1602829 (2017).
18. W. Li, M. Zhou, H. Li, K. Wang, S. Cheng, and K. Jiang, "A high performance sulfur-doped disordered carbon anode for sodium ion batteries." *Energy Environ. Sci.*, 8, 2916 (2015).
19. S. Zhang, T. P. Pollard, X. Feng, O. Borodin, K. Xu, and Z. Li, "Altering the electrochemical pathway of sulfur chemistry with oxygen for high energy density and low shuttling in a Na/S battery." *ACS Energy Lett.*, 5, 1070 (2020).
20. R. R. Mitchell, B. M. Gallant, Y. Shao-Horn, and C. V. Thompson, "Mechanisms of morphological evolution of Li2O2 particles during electrochemical growth." *J. Phys. Chem. Lett.*, 4, 1060 (2013).
21. B. M. Gallant, D. G. Kwabi, R. R. Mitchell, J. Zhou, C. V. Thompson, and Y. Shao-Horn, "Influence of Li2O2 morphology on oxygen reduction and evolution kinetics in Li–O2 batteries." *Energy Environ. Sci.*, 6, 8 (2013).
22. O. L. Cormac, M. Sanjeev, and K. M. Abraham, "Influence of nonaqueous solvents on the electrochemistry of oxygen in the rechargeable lithium-air battery." *J. Phys. Chem. C*, 114, 9178 (2010).
23. L. Guo, G. Oskam, A. Radisic, P. M. Hoffmann, and P. C. Searson, "Island growth in electrodeposition." *J. Phys. D*, 44, 443001 (2011).
24. J. Yang, B. J. McCoy, and G. Madras, "Distribution kinetics of polymer crystallization and the avrami equation." *J. Chem. Phys.*, 122, 064901 (2005).
25. A. Bewick, M. Fleischmann, and H. R. Thirsk, "Kinetics of the electrocrystallization of thin films of calomel." *Trans. Faraday Soc.*, 58, 2200 (1962).
26. S. M. Allen, R. W. Balluffi, and W. C. Carter, *Kinetics of Materials*, ed. R. A. Kemper (John Wiley & Sons, Inc, Cambridge) (2005).
27. F. Y. Fan, W. C. Carter, and Y. M. Chiang, "Mechanism and kinetics of Li2S precipitation in lithium-sulfur batteries." *Adv. Mater.*, 27, 5203 (2015).

28. Y. X. Ren, H. R. Jiang, T. S. Zhao, L. Zeng, and C. Xiong, "Remedies of capacity fading in room-temperature sodium-sulfur batteries." *J. Power Sources*, 396, 304 (2018).
29. Y. X. Ren, T. S. Zhao, M. Liu, P. Tan, and Y. K. Zeng, "Modeling of lithium-sulfur batteries incorporating the effect of Li2S precipitation." *J. Power Sources*, 336, 115 (2016).
30. R. Carter, A. NewRingeisen, D. Reed, R. W. Atkinson, P. P. Mukherjee, and C. T. Love, "Optical microscopy reveals the ambient sodium–sulfur discharge mechanism." *ACS Sustainable Chemistry & Engineering*, 9, 92 (2020).
31. F. Y. Fan, W. H. Woodford, Z. Li, N. Baram, K. C. Smith, A. Helal, G. H. McKinley, W. C. Carter, and Y. M. Chiang, "Polysulfide flow batteries enabled by percolating nanoscale conductor networks." *Nano Lett.*, 14, 2210 (2014).